



ELSEVIER

Available online at [www.sciencedirect.com](http://www.sciencedirect.com)

SCIENCE @ DIRECT®

C. R. Geoscience 336 (2004) 395–406



## Tectonics

# Drilling through the active Aigion Fault: the AIG10 well observatory

François H. Cornet <sup>a,\*</sup>, Mai Linh Doan <sup>a</sup>, Isabelle Moretti <sup>b</sup>, Günter Borm <sup>c</sup>

<sup>a</sup> Laboratoire de mécanique des roches, Institut de physique du Globe de Paris, 4, place Jussieu, 75252 Paris cedex 05, France

<sup>b</sup> Division Géologie–Géochimie, Institut français du pétrole, 1 et 4, av. de Bois-Préau, 92852 Rueil-Malmaison cedex, France

<sup>c</sup> Department of Geomechanics & Geotechnology, GeoForschungsZentrum Potsdam, Telegrafenberg A17,

14473 Gross Glienicker Potsdam, Germany

Received 5 February 2004; accepted 10 February 2004

Written on invitation of the Editorial Board

## Abstract

The 1000 m-deep AIG10 borehole intersects the Aigion Fault within the limestone of the Pindos nappe at 760 m. It has demonstrated that the fault is dipping 60° with respect to horizontal, an angle consistent with the strength characteristics of the fault material as determined in the laboratory. It does not seem to be listric, as suggested by the location of superficial microseismic events. The fault is about 7 m thick, with a 50 cm core of clay derived from smeared radiolarite formation. The fault offsets the basement rock by  $150 \pm 20$  m and constitutes a hydraulic barrier that sustains a 0.5 MPa differential pressure. Below the fault, a strongly karstified limestone has been encountered down to 1000 m. It is the site of a 0.9 MPa overpressure and exhibits no temperature gradient. Water geochemistry demonstrates the continental origin of this significant flow, which obliterates the regional heat flux. The present monitoring of downhole pressure yields data on tidal variations with a resolution of 1/500 as well as pressure variations induced by teleseisms. Given preliminary results from  $^{14}\text{C}$  dating, the age of the fault is about 50 kyr and the mean slip rate equal about 3.5 mm yr $^{-1}$ . **To cite this article:** F.H. Cornet et al., C. R. Geoscience 336 (2004).

© 2004 Académie des sciences. Published by Elsevier SAS. All rights reserved.

## Résumé

**Forage au travers de la faille active d'Aigion : l'observatoire constitué par le puits AIG10.** Le forage AIG10 recoupe la faille d'Aigion au niveau des carbonates de la nappe du Pinde, à 760 m de profondeur. Il a démontré que la faille présente un pendage de 60°, valeur conforme aux mesures de laboratoire quant au coefficient de frottement des matériaux prélevés dans la faille. Celle-ci ne semble pas listrique, d'après la localisation d'événements microsismiques dans le prolongement à 4 km de profondeur du plan de faille. Son épaisseur atteint 7 m, avec un cœur argileux de 50 cm d'épaisseur provenant de l'étirement des radiolarites, qui lui confère une certaine étanchéité. Celle-ci se manifeste par un différentiel de pression interstitielle de 0,5 MPa. Sous la faille, le forage recoupe un calcaire fortement karstifié, supportant une surpression interstitielle de 0,9 MPa par rapport à la valeur hydrostatique. L'analyse géochimique de l'eau démontre son origine continentale. L'absence de gradient thermique dans le karst, sous la faille, témoigne de l'existence d'un flux important, qui ne permet pas l'observation directe du flux de chaleur profond. Le rejet total de la faille est de  $150 \pm 20$  m, avec un taux de glissement moyen de 3,5 mm a $^{-1}$  pour un âge d'environ 50 ka, selon les premiers résultats de datation au  $^{14}\text{C}$ . **Pour citer cet article :** F.H. Cornet et al., C. R. Geoscience 336 (2004).

© 2004 Académie des sciences. Published by Elsevier SAS. All rights reserved.

\* Corresponding author.  
E-mail address: cornet@ipgp.jussieu.fr (F.H. Cornet).

**Keywords:** fault strength; clay smearing; friction law; Aigion fault offset; fault hydraulic property

**Mots-clés :** résistance de faille ; loi de frottement ; étirement des argiles ; rejet de la faille d'Aigion ; caractéristiques hydraulique

## Version française abrégée

### 1. Introduction

Il y une quinzaine d'années, le forage de Cajon Pass, à proximité de la faille de San Andrea, en Californie, a permis de confirmer l'absence de flux de chaleur anormal au voisinage de cette faille, alors que les lois de frottement obtenues au laboratoire laissaient penser le contraire [13,23]. Une des raisons invoquées serait une augmentation de pression interstitielle lors du processus de rupture. Depuis, un certain nombre de forages a été réalisé juste après certains séismes pour déterminer le profil thermique local et préciser ainsi les lois de comportement hydromécanique des failles.

L'objectif du forage AIG10, sur la faille d'Aigion dans le golfe de Corinthe, est précisément de mesurer en continu la pression interstitielle sous, dans, et au-dessus de cette faille active, avant, pendant et après un séisme. Il est aussi de préciser la morphologie et les caractéristiques hydromécaniques de cette faille. Il est enfin d'établir son rôle sur les écoulements régionaux, afin de déterminer si la faille joue le rôle de drain ou, au contraire, de barrière hydraulique.

### 2. Structure géologique locale

Tant les profils sismiques de reconnaissance initiale que les résultats du forage (analyse des *cuttings* et des 80 m de carottes obtenus dans et au voisinage de la faille, diagraphies d'imagerie électrique et ultrasonore, diagraphie sonique et profiles sismiques verticaux) permettent de préciser la structure géologique locale [6,15,18,20]. Après les sédiments argileux récents des 150 premiers mètres, le forage recoupe successivement des congolomérats indurés de 150 à 388 m, puis des dépôts argileux jaunâtres de 388 à 496 m, profondeur du contact avec les radiolarites de la nappe du Pinde. À 696 m, le forage pénètre dans les calcaires en plaquettes caractéristiques du sommet de la série du Pinde, avant de recouper la faille d'Aigion à 758 m. De 780 à 1001 m, le forage recoupe un calcaire homogène localement karstifié (Fig. 1).

Il apparaît ainsi que la faille présente un pendage de 60°, qu'elle semble conserver jusqu'à son enracement dans la zone sismogénique profonde (6–8 km), si l'on en juge par la localisation d'événements micro-sismiques observés vers 4 km de profondeur. Son rejet a été évalué à  $150 \pm 20$  m, grâce aux diagraphies soniques, aux profils sismiques verticaux et aux profils sismiques de reconnaissance, qui permettent de bien évaluer le rejet des calcaires (vitesse de  $5 \text{ km s}^{-1}$ ) et du toit des radiolarites (vitesse de  $3600 \text{ m s}^{-1}$ ). L'âge de la faille serait d'environ 50 ka d'après le rejet entre un niveau daté à 35 ka et identifié à 103 m de profondeur dans le compartiment nord et une terrasse caractéristique du niveau de la mer il y a 38 ka, identifiée à 30 m au-dessus du niveau de la mer actuel dans le compartiment sud [14,15]. Cet âge impliquerait donc une vitesse de glissement moyen de  $3,7 \text{ mm an}^{-1}$ , en bon accord avec les estimations faites à partir des anciennes terrasses marines [7]. Toutefois, la datation de la terrasse aurait été récemment remise en cause et l'âge reste donc encore à confirmer.

### 3. Morphologie de la faille et caractéristiques hydromécaniques

La faille telle qu'elle a été recoupée par le forage de 756 à 772,5 m est constituée d'une brèche calcaire de 772,5 à 762,5 m, puis d'une couche argileuse de 1 m d'épaisseur, elle-même surmontée d'une brèche calcaire de 761,5 à 756 m. Ainsi, du fait de son pendage de 60°, la faille présente une épaisseur totale de 7 m, dont 50 cm d'argile dont la composition siliceuse démontre qu'elle provient de la déformation d'un niveau de radiolarite. Les mesures de laboratoire [21,22] montrent que le coefficient de frottement dans l'argile est de 28 à 29° et celui des surfaces de glissement dans la brèche de 32°. Ces valeurs sont donc tout à fait homogènes avec l'orientation moyenne de la faille, mais l'orientation des plans de glissement interne montre que les mécanismes de déformation à l'intérieur de la faille sont plus complexes qu'un simple glissement plan (Fig. 2). Il a été montré que la

perméabilité de l'argile varie entre 1 et  $20 \times 10^{-19} \text{ m}^2$ , selon la contrainte moyenne appliquée.

L'analyse géochimique de l'eau dans les divers aquifères montre une influence marine forte dans les terrains quaternaires jusqu'à 388 m de profondeur, mais les eaux prélevées à partir de 700 m de profondeur sont d'origine continentale, sans aucune influence marine. L'observation d'une pression de 5 bar dans les calcaires au-dessus de la faille et de 8,5 bar dans le karst profond démontre, d'une part, le rôle de barrière hydraulique de la faille, mais aussi l'influence de la couverture de radiolarite et des argiles anciennes de la base du Quaternaire quant à l'hydrogéologie régionale. Par ailleurs, l'absence de gradient thermique (température de 31,5 °C de 750 à 995 m, Fig. 3) dans les calcaires karstiques profonds témoigne d'une circulation rapide qu'il reste à préciser. En revanche, tant l'existence d'un gradient thermique continu que les figures de cristallisation calcique démontrent l'absence de circulation rapide dans les calcaires au-dessus de la faille.

#### *4. Résultats préliminaires quant aux variations de pression interstitielle sous la faille*

Des premiers essais de production d'eau, réalisés lorsque l'instrument de forage était encore en place, mais après la cimentation d'un cuvelage ancré à 708 m de profondeur dans le calcaire à plaquettes [10], ont mis en évidence un débit de production d'environ  $50 \text{ m}^3 \text{ h}^{-1}$  dans les calcaires karstiques profonds. Mais, lors de la mise en place du matériel de surveillance permanent, alors que le forage était entièrement libre, les débits de production se sont révélés supérieurs à  $500 \text{ m}^3 \text{ h}^{-1}$  et ont peut être atteint  $600 \text{ m}^3 \text{ h}^{-1}$  d'après la vitesse de remplissage d'un réservoir tampon de  $2000 \text{ m}^3$  construit pour ces essais. Ces premières observations fournissent une valeur minimum de l'ordre de  $10^{-5} \text{ m s}^{-1}$  pour la conductivité hydraulique du karst. Ces valeurs seront précisées à partir de l'analyse des variations de pression induites tant par les marées que par les télésismes (Figs. 4, 5 and 6).

## 1. Introduction

Some fifteen years ago, the debate on the stress/heat flux paradox [13,23] illustrated the discrepancy that

still exists today between the mechanical behaviour of major faults as estimated from laboratory experiments and that derived from observations conducted in deep boreholes. The most conspicuous difference is the absence of abnormal heat flux close to the San Andreas Fault (California), while the shear strength deducted from laboratory-derived friction laws implies large generation of heat. The Cajon Pass Scientific Drilling Project involved the drilling of a 3.5 km deep well that provided various in situ observations, including the confirmation of the absence of heat anomaly close to the fault at depth. It also showed that, on this site, the principal stress directions are nearly perpendicular and parallel to the fault, so that the fault supports very little shear stress. This has led to the conclusion that the San Andreas Fault is 'weak' and various mechanisms have been proposed to explain why faults may be 'strong', i.e., basically follow Byerlee's law, or may be weak, i.e., support very little shear stress.

A key parameter is the interstitial pore pressure that exists within the fault during rupture, whether this rupturing process is slow (creeping) or of seismic nature. But no data are yet available on the pore pressure conditions that exist in faults at depth and various deep borehole projects have been undertaken to provide a better understanding of these pressure conditions. Most of them involve drilling through seismogenic faults, just after an earthquake has occurred. This provides means to evaluate the local thermal and stress conditions associated with the failure process. One of the objectives of the Aigion drilling project is to provide data on the pore pressure conditions that exist before, during, and after an earthquake within the active Aigion Fault. Indeed, the Aigion Fault was slightly reactivated during the magnitude-6.2 Aigion earthquake that occurred in 1995 on a low dipping offshore fault [3,12]. Investigating the present-day fluid flow and temperature conditions on this fault will bring information on the healing process that might affect the fault.

A second objective of the Aigion Fault drilling project is to determine the role of Aigion Fault in the regional hydro-geological flow conditions. Indeed, faults may act either as fluid conduits or as flow inhibitors. For example, in the Monterrey Basins, in California, faults are efficient conduits in low-permeability siliceous rocks [8], but retard fluid flow in high-permeability sandstones [1]. So-called sealing

faults have drastic influences on the pressure distribution in hydrocarbon reservoir [11] and a better understanding on the role of clay on the hydromechanical behaviour of faults, in particular the clay-smearing effect within carbonate rocks, is of great importance for the oil industry [2].

The AIG10 borehole has been designed to provide data on the Aigion Fault morphology and its hydro-mechanical properties at depths where it intersects the Mesozoic formation below the Quaternary deposits. It is also meant to provide means for continuously monitoring both the deformation process and the various fluid fault interactions, including hydro-thermo-mechanical coupling effects and also physicochemical interactions on sealing effects.

This paper summarizes results obtained by the drilling of the AIG10 well. They concern the regional geological structure, including the dip and offset of Aigion Fault, as well as the fault morphology and its influence on regional flow. Finally, preliminary results on the monitoring of pore pressure below the fault are presented. More detailed information on these various results may be found in the corresponding papers presented in this special issue.

## **2. The local geological structure**

Before drilling the AIG10 well, a preliminary seismic reconnaissance was undertaken for a precise site selection [18]. Then, during drilling, cuttings were collected every 2 m, except from 708 to 787 m, where continuous coring was undertaken in order to obtain a petrographic characterisation of the fault material within the Pindos unit (a sedimentary formation made up of intercalations of carbonate rocks and radiolarite [9]). In addition, geophysical logs, including borehole imaging and sonic logs as well as vertical seismic profiles, were completed. This has provided material for a detailed lithological and structural investigation of the formations intersected by the well [6,18,20]. Results are summarized in Fig. 1.

On the vertical seismic profiles, the top of the limestone ( $5 \text{ km s}^{-1}$  P-wave velocity) is outlined in the southern footwall by a strong diffraction [18]. The transition from the basal Quaternary clay to the tectonised Pindos unit is identified at 496 m from the lithological log, but the top of basement rocks is iden-

tified only at 520 m from sonic and VSP logs. This means that the upper layers of the Pindos unit intersected by the well cannot be identified by their velocity contrast. Only the limestone layers some 25 m lower than the interface have a velocity contrast of significance that can be identified in the seismic profiles. These limestone layers are identified at a 420 m depth some 1.5 km to the south of the fault surface trace, on the seismic profile run during the initial seismic reconnaissance along a north-south direction passing through the well site. This depth is determined from the refraction analysis with velocity values for the upper Quaternary formation taken equal to the values identified by the VSP run in AIG10. Hence, if one assumes a  $4^\circ$  dip toward the south for this interface, this yields a depth of 370 m for these limestone layers at their intersection with the fault, in the southern footwall. This implies a 350 m depth for the interface between the basal Quaternary clay and the radiolarite, in the footwall. Such a value would then fit with the 150 m offset derived from the offset of the platy limestone encountered at 696 m in the northern hanging wall of the fault. Thus, the vertical offset of the fault is well constrained by the displacement of the basal formation and is found to be equal to  $150 \pm 20$  m. In the Quaternary formation, the top of the stiff conglomerates is identified at 153 m by Lemeille et al. [15] from the lithological log, but at 127 m from the VSP velocity profile. This implies that the top of the stiff conglomerates, on the southern footwall, is encountered below present-day sea level, and therefore do not contribute to the present-day local geomorphology.

The mean dip of the fault is also very well constrained by the fault outcrop near the railway track and the fault intersection with the well at 760 m depth. Interestingly, this dip is consistent with the location of a few microseismic events observed between 3.5 and 4 km [4]. It is found to be equal to  $61 \pm 2^\circ$ , so that the fault total slip is about 173 m. Given that the fault extension is in the order of 10 km [19], the total fault slip over fault length ratio is equal to about 0.017, a value very consistent with those obtained by Manighetti et al. [16] in the Afar Rift for a collection of 255 faults. Hence, this work suggests that the fault dip remains constant at depth, till the fault reaches the low dipping regional seismic zone between 4 and 8 km. These observations therefore suggest that the Aigion Fault may not be listric.

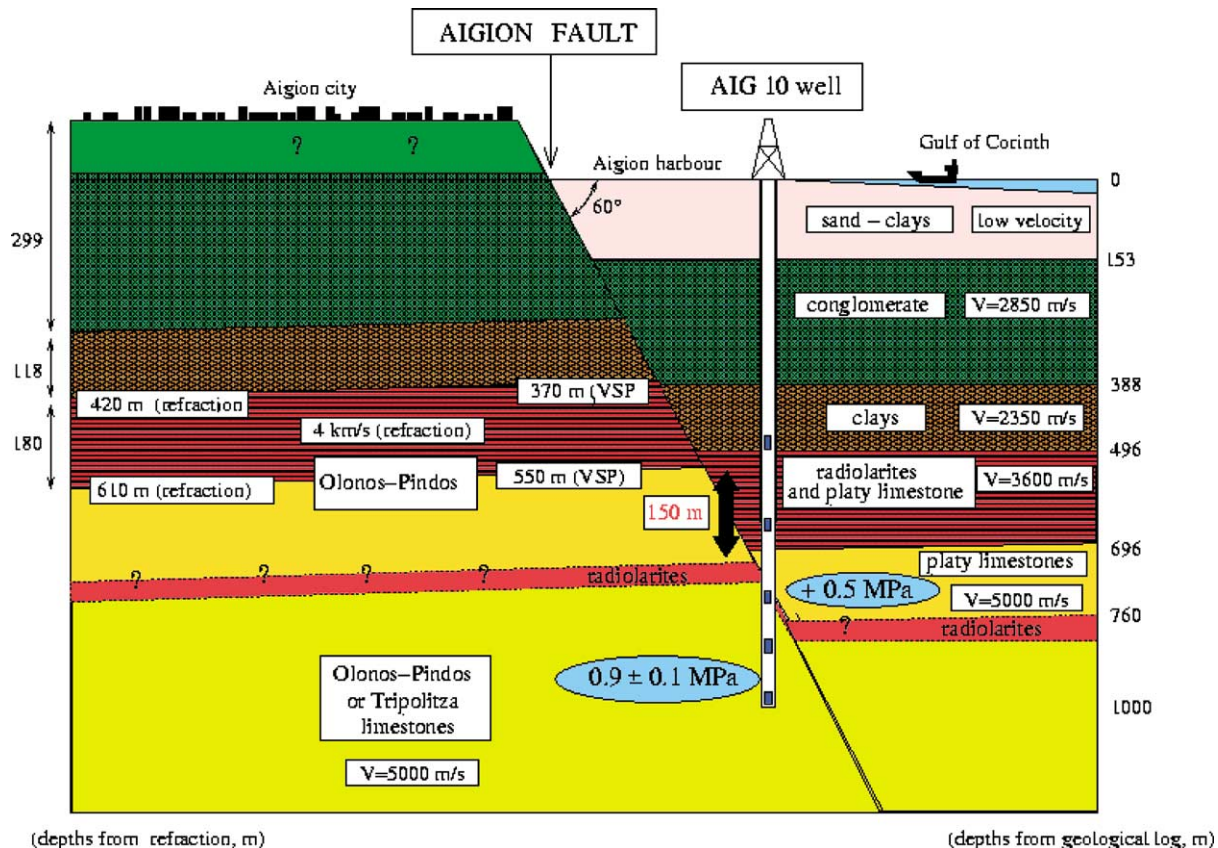


Fig. 1. Schematic structural cross section through Aigion Fault, in the Aigion harbour. On the left, depths have been estimated from seismic refraction data [18], while on the right depths correspond to cuttings and core analysis [15,20]. Velocities indicated on the right part of the figure correspond to P wave arrivals from sonic logs, while on the left part velocities are those estimated from seismic refracted data. Note the slow velocity within the calcareous clays (calicitite) below the conglomerates. The red layer corresponds to a radiolarite clayish layer smeared through the fault, as explained in Section 3. Its thickness and lateral extension is unknown. The pore pressure values correspond to measurements obtained during the drilling phase for the platy limestone and after drilling operation for the limestone encountered below the fault. The fault offset is determined from the offset of the platy limestone (layer with  $V_p$  velocity equal to  $5 \text{ km s}^{-1}$ ) and from that of the radiolarite–Quaternary clay interface.

Fig. 1. Schéma structural de la faille d'Aigion, au niveau du port d'Aigion. À gauche de la figure, les profondeurs sont estimées à partir des données sismiques [18], tandis qu'à droite, elles résultent d'observations lithologiques dans le forage [15,20]. Les vitesses indiquées sur la partie droite de la figure concernent les ondes P des diagraphies soniques, tandis que les valeurs sur la gauche proviennent de l'analyse des données de sismique réfraction. On remarquera la couche lente entre les conglomérats et les radiolarites. Le niveau rouge correspond à un niveau de radiolarites à l'origine des argiles au cœur de la faille, son épaisseur et son extension latérale étant inconnues. Le rejet de la faille a été déterminé à partir des données sismiques concernant le toit des radiolarites et surtout le calcaire ( $V_p = 5 \text{ km s}^{-1}$ ).

Cuttings from a well located midway between AIG10 and the fault outcrop show no tilting of the Quaternary sediments in the northern hangingwall. This absence of tilt is confirmed by correlation between the cuttings from various nearby boreholes located some 2 to 3 km from AIG10 [15]. But Mesozoic basement rocks have been strongly deformed dur-

ing the Hellenides compression, so that the Mesozoic structures are not horizontal any longer. The structural data retrieved from borehole images [6] indicate that sedimentary layers in the platy limestone above 744 m are dipping 45° toward the east, while they are plunging 45° to the southeast, between 744 m and Aigion Fault. Hence, the subhorizontal contact that is derived

from the seismic profiles corresponds solely to the interface between basement rocks and Early Quaternary deposits. This work does not resolve the structure within the basement rock at a scale larger than that of AIG10 well because of the strong heterogeneity in the deformation.

The dating of the fault is provided by the offset of Quaternary formations. A terrace dated 38 kyr from  $^{14}\text{C}$  dating is identified 30 m above sea level (a.s.l.) on the southern footwall [14], while sediments dated 35 kyr also by  $^{14}\text{C}$  dating are encountered at 103 m depth (b.s.l.), on the northern hangingwall [15]. Given the fact that the sea was not deeper than 5 to 10 m when this formation was deposited, this would suggest that the fault vertical offset generated since 35 kyr is close to 120 m and therefore that the mean vertical slip rate, for this period, is in the order of  $3 \text{ mm yr}^{-1}$ , or a mean total slip rate of  $3.5 \text{ mm yr}^{-1}$ , a value quite consistent with that determined from palaeoseismological investigations [19]. Given the usual assumption of 1/3 up and 2/3 down for motion on normal faults with  $60^\circ$  dip angle, this would result in an uplift rate of the southern footwall of Aigion Fault equal to about  $1 \text{ mm yr}^{-1}$ . This result is also in agreement with estimates from uplifted terraces analysis [7]. It may be mentioned however that recent observations (Lemeille personal communication), would seem to indicate that the  $^{14}\text{C}$  age proposed for the terrace observed 30 m a.s.l. is erroneous and that the fault may be older. Pending further published results on the dating of terraces and Quaternary layers, it is concluded here that the Aigion Fault is at least 50 kyr old, but possibly older.

### 3. The Aigion Fault morphology and its role as hydraulic barrier

At its intersection with the Aigion Fault, the well AIG10 is vertical ( $3^\circ$  inclination with respect to vertical). The fault material, as seen from cores and geophysical logs, consists of 9 m of brecciated limestone surmounted by 1 m of clay, itself surmounted by 3 m of heavily brecciated limestone [6]. Hence given its  $60^\circ$  dip, the fault is found to be about 7 m thick with a 50 cm core of clay. The particle size distribution for the fault clay material shows a large range of particle sizes [22]. It consists mostly of siliceous ma-

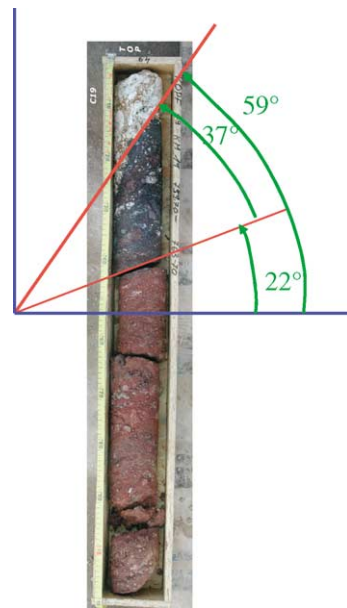


Fig. 2. Core retrieved from the clay zone, at 760 m in well AIG10. Note the inclination of the slip plane between red and grey clay zones with respect to that of the contact between the clay zone and the breccias.

Fig. 2. Carotte prélevée dans l'agile qui constitue le cœur de la faille, à 760 m de profondeur. On remarquera la différence d'inclinaison du contact entre l'argile et la brèche, d'une part, entre le contact séparant l'argile noire de l'argile rouge, d'autre part. Ce dernier plan présentait des stries très marquées.

terial [21]. Hence the presence of clay results mostly from the smearing of the radiolarite formation rather than from the wearing of the carbonate fault walls.

The clay zone makes an angle of  $31^\circ$  with respect to the borehole axis. Inside the clay zone, a shearing surface with marked slip lines is visible on a plane that makes a  $68^\circ$  angle with respect to the core axis (Fig. 2). In addition, within the calcitic brecciated zone, slip zones with clear slip lines are also visible. This shows that slip occurs within both the clay zone and the calcitic breccia. Both the mechanical and hydraulic properties of these materials have been investigated in the laboratory [21,22]. The permeability of the clay is found to vary with stress and ranges from  $0.1$  to  $2 \times 10^{-18} \text{ m}^2$ . The friction angle of the clay is equal to  $28^\circ$  at room temperature ( $22^\circ\text{C}$ ), but increases to  $29^\circ$  when the temperature increases to  $73^\circ\text{C}$ . The clay has been shown to exhibit a contractant volumetric behaviour, when heated. The joint

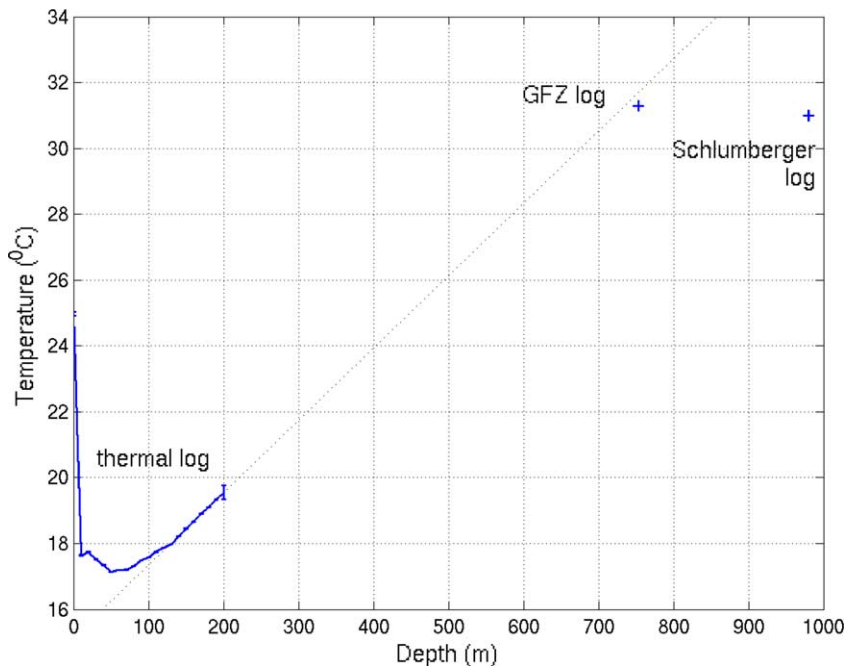


Fig. 3. Temperature profile in well AIG10. The continuous profile was obtained 9 months after the well had been drilled, when it was filled with heavy mud. The thermistance was too light to reach deeper than 200 m. The measurement at 749 m was also obtained 9 months after the end of drilling by optic cable (courtesy of A. Forster, GFZ). The measurement at the bottom of the well was obtained three days after the end of drilling and therefore likely yields a slight underestimate.

Fig. 3. Profil thermique dans le forage AIG10. Le profil continu, jusqu'à 200 m de profondeur, a été obtenu 9 mois après la réalisation du forage. Le trop faible poids de la thermistance ne lui a pas permis de descendre plus profondément, étant donné la densité de la boue de remplissage utilisée pour stabiliser la pression interstitielle en dessous de 760 m. La mesure à 749 m a été obtenue par GFZ-Potsdam, à l'aide d'une fibre optique, onze mois après la fin du forage, alors que ce dernier était encore stabilisé par la boue (A. Forster, GFZ, communication personnelle). La mesure au fond du forage a été obtenue par la société Schlumberger, une semaine après la fin du forage. Elle ne devrait pas être perturbée de façon très significative par l'opération de forage, étant donné qu'elle a été effectuée au fond du forage.

between the carbonate zone and the cataclastic bands, oriented  $112^\circ$  with respect to the core axis, shows a residual friction angle equal to about  $32^\circ$ , i.e., only slightly larger than that of the clay. Hence, at a large scale, the observed  $60^\circ$  dip angle for the Aigion Fault is completely consistent with the measured friction angle for the clay and the interface between cataclastic zone and intact rock, if the vertical direction is the maximum principal stress direction. Yet, the orientations of observed slipping surfaces within the fault suggest a more complex deformation mechanism, at the meter scale.

Water-geochemistry analysis [10] shows that while the water in the Quaternary conglomerates exhibits a strong marine component, that present in the carbonate formation, below the radiolarite, is of meteoritic origin. It has been recharged in regions south of Aigion.

Below the radiolarite formations, the fault separates two different aquifers. In the upper one, a 0.5 MPa over hydrostatic pressure was measured during the drilling operation, while below the fault the overpressure reaches 0.85 MPa, as monitored during two months in fall 2003. Hence the fault is found to be a strong hydraulic barrier. A pumping test conducted between 708 and 744.8 m in the upper platy limestone formation yields a hydraulic conductivity equal to about  $1 \times 10^{-7} \text{ m s}^{-1}$  [10], if one assumes that flow occurs in the fracture network, as suggested by laboratory permeability measurements for the intact platy limestone [21]. But flow conditions below the fault are completely different. First, imaging logs have revealed the existence of numerous karstified fractures with open sections as large as 1 m. Second, various temperature measurements and thermal log yields a

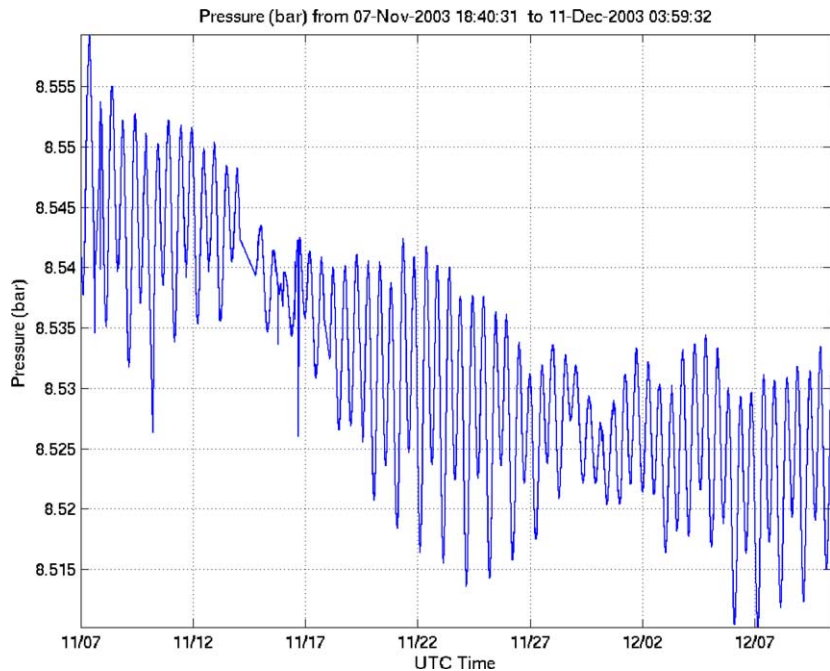


Fig. 4. Signal recorded by the pressure transducer in AIG10 borehole during fall 2003 and showing tidal pressure variations.

Fig. 4. Variations de pression en dessous de 700 m, dans le forage AIG10. Le forage est rempli d'eau et les deux compartiments de part et d'autre de la faille sont en communication. La mesure correspond à la pression dans le karst profond, du fait de la forte impédance hydraulique des calcaires au-dessus de la faille.

$23^\circ/1000$  m gradient from 120 m down to the fault but a uniform temperature below the fault, down to the bottom of the well (Fig. 3). The absence of thermal gradient below the fault testifies for an active flow that remains to be properly characterized.

Whether the karstification process is still active or whether it occurred prior to the opening of the rift remains also to be determined. In the latter case, this would imply a downward displacement of the Aigion footwall limestones larger than 1000 m and therefore a total cumulated differential vertical offset larger than 1500 m for the whole rifting process. Interestingly, Quaternary conglomerates are identified at altitudes larger than 700 m at Fteri, some 8 km south of Aigion. Hence, at this point, it is not clear whether the karst developed in unsaturated conditions, when the formation was above sea level or whether it is still developing under water saturated conditions. The important conclusion is that today, the Aigion Fault together with the tectonized radiolarites of the Pindos unit prevent water infiltrated in the mountainous range south of Aigion from reaching ground surface. This

regional flow dominates the regional thermal gradient and pre-empts direct regional heat flux measurements.

#### 4. Preliminary results from the downhole pore-pressure monitoring

A still pending critical question is the characterization of the flow within the karstified limestone below the fault. A first test of water production was undertaken at the end of drilling, when the drill rig was still on site but after a tube had been cemented down to 711 m into the platy limestone above the fault. The flow-rate measured during the three days of the test oscillated around  $50 \text{ m}^3 \text{ h}^{-1}$  with no noticeable decrease of flow, but the flow carried a significant proportion of cuttings. It was found later that in fact the flow was obstructed by these cuttings accumulated near the drill bit left in the well. Indeed, after the well site had been equipped with a water evacuation system dimensioned to accommodate the expected  $50 \text{ m}^3 \text{ h}^{-1}$  flow-rate, the well was left open to flow freely. The

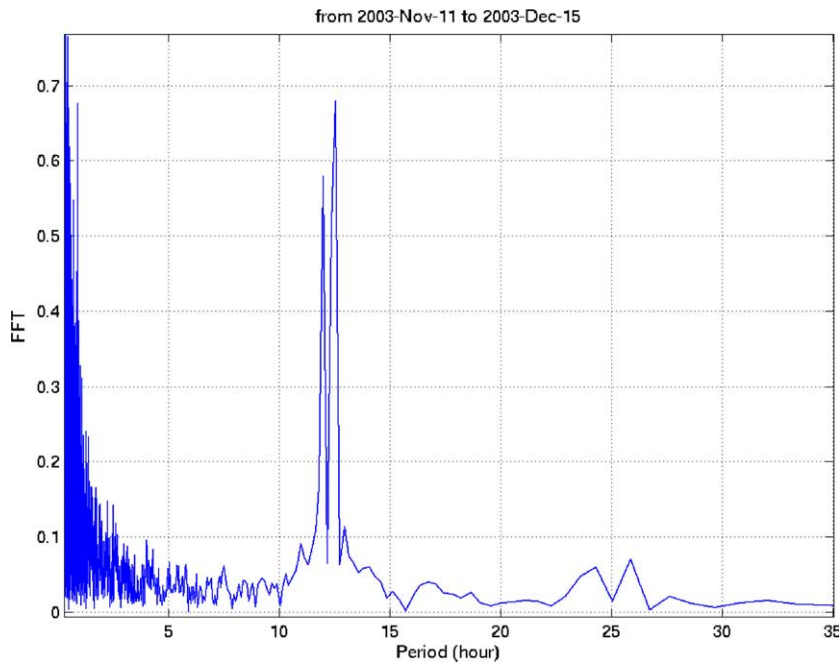


Fig. 5. Spectral analysis of the pressure signal of Fig. 4. Semi-diurnal waves are predominant over diurnal waves.

Fig. 5. Analyse spectrale des variations de pression enregistrées sous la faille. On relève le caractère prédominant des ondes semi-diurnes.

production flow increased progressively and reached values larger than  $500 \text{ m}^3 \text{ h}^{-1}$  after two days and got possibly as high as  $600 \text{ m}^3 \text{ h}^{-1}$ . This was measured by the time required to fill up a temporary  $2000 \text{ m}^3$  storage pond constructed for this purpose. If one assumes an equivalent porous material over a  $250 \text{ m}$  height with a  $500 \text{ m}$  influence radius for the well, this would result in a hydraulic conductivity equal to  $1.1 \times 10^{-5} \text{ m s}^{-1}$  ( $1.5 \times 10^{-5} \text{ m s}^{-1}$  for a  $10000 \text{ m}$  influence radius), according to Dupuit equation for stationary flow in confined aquifers (see, e.g., [17]). This value is clearly an underestimate, given the existence of a few localized karstified fractures. This shows that the hydraulic conductivity below the fault is nearly two orders of magnitude larger than that of the platy limestone above the fault, and possibly more.

Unfortunately, this very high production flow rate prevented the installation of packers at the proper depths in the well so that the pressure presently monitored when the wellhead is closed yields the downhole pressure. This monitoring is conducted with various sensors. The most sensitive of them records absolute pressure at the rate of  $0.125 \text{ Hz}$  with a resolution of  $5 \text{ Pa}$ . Fig. 4 displays the data

recorded during fall 2003. A complementary pressure transducer yields the same variations, but with a much coarser resolution.

The long-term trend and tidal variations are shown in Fig. 4. Given the contrast in transmissivity of the upper and lower compartments on both sides of the fault, pressure variations are dominated by those of the lower karstic zone. Tidal waves are visible with a resolution of  $1/500$ . A spectrum analysis over one month of recorded data is sufficient to distinguish between M2 (12.42 h) and S2 (12 h) semi-diurnal waves, as presented in Fig. 5. Diurnal waves are also identified but with lower intensity. The high amplitude of the tides ( $\sim 25 \text{ mbar}$ ) shows the sensitivity of the aquifer to the marine tides in the Corinth Gulf. The response of the aquifer to tidal and barometric loading is currently under investigation, to determine the hydraulic characteristics of the aquifer.

The high sensitivity of the pressure transducer also enables it to record seismic waves. During September and November 2003, two major earthquakes occurred in Hokkaido and the Aleutian Islands, with magnitudes larger than 8. The Aleutian Islands signal is displayed in Fig. 6 together with the theoretical times

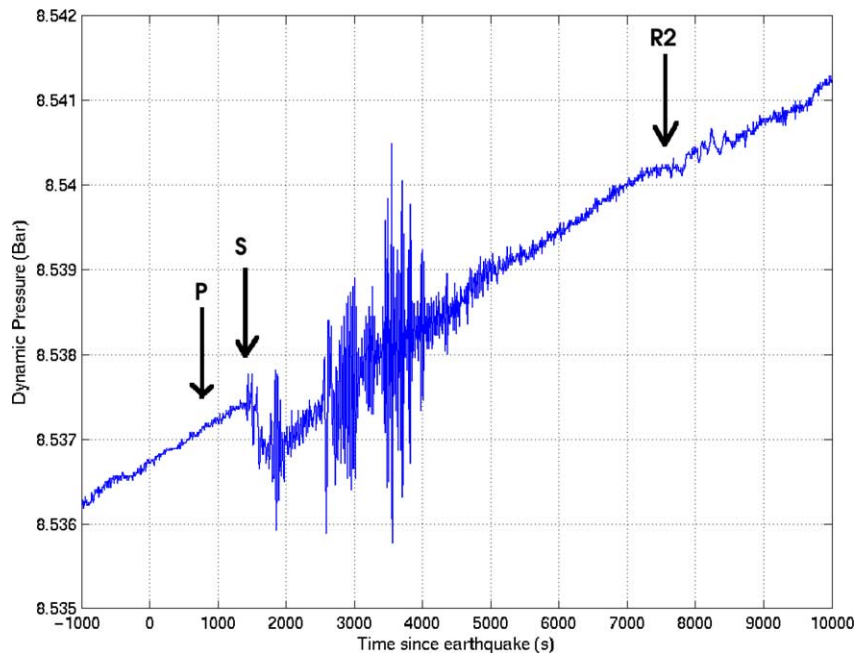


Fig. 6. Teleseismic signal recorded with the pressure transducer in AIG10 on 17 November 2003, near 7 AM, UTC time. The earthquake occurred in the Aleutian isles at 6 h 43. Theoretical arrival times of P, S and the first major arc Rayleigh waves (R2) are indicated. Note the drop in pressure concomitant with S waves arrival.

Fig. 6. Signal télésismique enregistré avec le capteur de pression de AIG10, le 17 novembre 2003, vers 7 h 00 du matin (temps d'origine du séisme intervenu dans les îles Aléoutiennes : 6 h 43). Les temps d'arrivée théorique des ondes P, S et de l'onde R2 de Rayleigh sont indiqués. On remarquera la chute de pression concomitante à l'arrivée des ondes S.

of arrival for volume waves and Rayleigh wave (the most rapid of surface waves). P waves are not noticeable, whereas S waves are clearly identified. This may appear surprising, since pressure changes are correlated to variation in rock pore volume and are therefore more sensitive to compressional waves. But in fact, the low sampling rate of the sensor filters out the high frequency P waves and detects S waves because of the S-to-P conversion at the surface near the borehole. The sensor is strongly responsive to surface waves whose periods (50–200 s) are best sampled by the sensor. Also, surface waves travelling around the globe are also visible 8000 s after the event. The drop in pressure simultaneous with the S wave arrival needs to be better documented. Indeed, similar effects of surface waves on quasistatic water-level variations have already been described at other sites [5]. In the present example, the abrupt character of the drop does not seem compatible with resonances of gulf water induced by windy weather. Indeed, the periods of these oscillations are

known to range from 8 to 40 min, and therefore seem to be out of the frequency domain of the observed perturbation. Ongoing work is being conducted to better understand this possible correlation.

## 5. Conclusion

Preliminary seismic reconnaissance, together with results from the drilling of the 1000 m-deep AIG10 well, has provided data that constrain the geometry and morphology of Aigion Fault. The fault is dipping 60° with respect to horizontal, an angle consistent with the strength characteristics determined in the laboratory, and does not seem to become listric at depth. It offsets the Mesozoic formation by about 150 m, with an average slip rate in the order of  $3.5 \text{ mm yr}^{-1}$ .

The fault, together with the radiolarite formation, has been shown to be a strong hydraulic barrier because of radiolarite clay smearing. Below the fault

encountered at 760 m, AIG10 intersects a well developed karst, which is the site of a 0.9 MPa overpressure resulting from infiltration in the mountain range more than 10 km south of Aigion. This downward flow completely obliterates any anomalous deep regional heat flux effects. Present monitoring of the pore pressure shows daily variations in the order of 2 kPa, which are generated by tides. This monitoring also provides an opportunity to investigate pore-pressure variations induced by both teleseismic and local earthquakes. These data will be taken advantage of for characterizing the hydraulic characteristics of the karst.

### Acknowledgements

All work conducted in connection with the AIG10 borehole was supported by European Commission contracts DGLab (EVR1-CT-2000-40005) and 3F-Corinth (ENK6-CT-2000-00056), by the International Continental Drilling Program, by the French ‘Centre national de la recherche scientifique – GDR Corinthe’ and by the German Research Foundation (DFG). The downhole monitoring equipment was developed with the help of Division Technique – INSU. Particular thanks are addressed to R. Verhille, C. Brunet, and B. Bert for their help during all phases of equipment preparation and testing and for their efficiency during all fieldwork. The assistance of F. Fontbonne during the deployment of equipment on site is also acknowledged.

### References

- [1] M. Antonellini, A. Aydin, Effect of faulting on fluid flow in porous sandstones: petrophysical properties, *Am. Assoc. Pet. Geol. Bull.* 78 (1994) 355–377.
- [2] A. Aydin, Y. Eyal, Anatomy of a normal fault with shear smearing: implications for fault seal, *Am. Assoc. Pet. Geol. Bull.* 86 (8) (2002) 1367–1381.
- [3] P. Bernard, P. Briole, B. Meyer, H. Lyon-Caen, J.-M. Gomez, C. Tiberi, C. Berge, R. Catin, D. Hatzfeld, C. Lachet, B. Lebrun, A. Deschamps, F. Courboulex, C. Laroque, A. Rigo, D. Massonet, P. Papadimitriou, J. Kassaras, D. Diagouras, K. Makropoulos, G. Veis, E. Papazisi, C. Mitsakaki, V. Karakostas, P. Papadimitriou, D. Papanastassiou, G. Chouliaras, G. Stavrakakis, The  $M_s = 6.2$ , June 15, 1995 Aigion Earthquake (Greece): evidence for low angle normal faulting in the Corinth Rift, *J. Seismol.* 1 (1997) 131–150.
- [4] P. Bernard, H. Lyon-Caen, P. Briole, A. Deschamps, K. Pitiakis, M. Manakou, F. Boudin, C. Berge, K. Makropoulos, D. Diagouras, P. Papadimitriou, F. Lemeille, G. Patau, H. Biliris, H. Castarèdes, J. Zaradnik, S. Sacks, A. Linde, Seismicity, deformation and seismic hazard in the western rift of Corinth: new insights from the Corinth Rift Laboratory (CRL), Tectonophysics, submitted for publication.
- [5] E.E. Brodsky, E. Roeloffs, D. Woodcock, I. Gall, M. Manga, A mechanism for sustained groundwater pressure changes induced by distant earthquakes, *J. Geophys. Res. B* 108 (8) (2003), ESE7.
- [6] J.-M. Daniel, I. Moretti, L. Micarelli, S. Essautier-Chuyné, C. Delle Piane, Macroscopic structural analysis of AIG10 well (Gulf of Corinth, Greece), *C. R. Geoscience* 336 (2004) 435–444, this issue.
- [7] P.M. De Martini, D. Pantosti, N. Palyvos, F. Lemeille, L. McNeil, R. Collier, Slip rates of the Aigion and Eliki faults from uplifted marine terraces, Corinth Gulf, Greece, *C. R. Geoscience* 336 (2004) 325–334, this issue.
- [8] S.K. Dholakia, A. Aydin, D.D. Pollard, M.D. Zoback, Fault controlled hydrocarbon pathways in the Monterey Formation, California, *Am. Assoc. Pet. Geol. Bull.* 82 (1998) 1551–1574.
- [9] T. Doutsos, G. Piper, K. Boronkey, I.K. Koukouvelas, Kinematics of the Central Hellenides, *Tectonics* 12 (1993) 936–953.
- [10] V. Giurgea, D. Rettemmaier, L. Pizzino, I. Unkel, H. Hötzl, A. Förster, F. Quattrocchi, Preliminary hydrogeological interpretation of the Aigion area from the AIG10 borehole data, *C. R. Geoscience* 336 (2004) 467–475, this issue.
- [11] R.J. Knipe, G. Jones, Q.J. Fisher, Faulting, fault sealing and fluid flow in hydrocarbon reservoirs: an introduction, in: G. Jones, Q.J. Fisher, R.J. Knipe (Eds.), *Faulting, Fault Sealing and Fluid Flow in Hydrocarbon Reservoirs*, in: *Geol. Soc. Spec. Publ.*, vol. 147, 1998, pp. 1–25.
- [12] I.K. Koukouvelas, The Egion fault, earthquake related and long term deformation, Gulf of Corinth, Greece, *J. Geodyn.* 26 (1998) 501–513.
- [13] A.H. Lachenbruch, J.H. Sass, Heat flow from Cajon Pass, fault strength, and tectonic implications, *J. Geophys. Res.* 97 (B4) (1992) 4995–5015.
- [14] F. Lemeille, D. Sorel, C. Bourdillon, C. Guermet, M. Manakou, C. Berge-Thierry, Quantification de la déformation associée à la faille active d’Aigion (golfe de Corinthe, Grèce) par l’étude des dépôts du Pléistocène supérieur et de la transgression marine holocène, *C. R. Geoscience* 334 (2002) 497–504.
- [15] F. Lemeille, F. Chatoups, M. Foumelis, D. Rettemmaier, I. Unkel, L. Micarelli, I. Moretti, C. Bourdillon, C. Guermet, C. Müller, Recent syn-rift deposits in the hangingwall of the Aigion Fault (Gulf of Corinth, Greece), *C. R. Geoscience* 336 (2004) 425–434, this issue.
- [16] I. Manighetti, G.C.P. King, Y. Gaudemer, C.H. Scholz, C. Doubre, Slip accumulation and lateral propagation of active normal faults in Afar, *J. Geophys. Res.* 106 (2001) 13667–13696.
- [17] G. de Marsily, *Hydrogéologie Quantitative*, Masson, Paris, 1981, p. 121.
- [18] C. Naville, S. Serbutoviez, I. Moretti, J.-M. Daniel, A. Throo, F. Girard, A. Sotiriou, A. Tselenitis, C. Skarpelos, C. Brunet,

- F.H. Cornet, Pre-drill surface seismic in vicinity of AIG10 well and post drill VSP, *C. R. Geoscience* 336 (2004) 407–414, this issue.
- [19] D. Pantosti, P.M. De Martini, I. Koukouvelas, L. Stamatopoulos, N. Palyvos, S. Pucci, F. Lemeille, S. Pavlides, Palaeoseismological investigations of the Aigion Fault (Gulf of Corinth, Greece), *C. R. Geoscience* 336 (2004) 335–342, this issue.
- [20] D. Rettenmaier, V. Giurgea, H. Hötzl, A. Förster, The AIG10 drilling project (Aigion, Greece): interpretation of the litholog in the context of regional geology and tectonics, *C. R. Geoscience* 336 (2004) 415–423, this issue.
- [21] I. Song, S.C. Elphick, N. Odling, I. Main, B.T. Ngwenya, Hydro-mechanical behaviour of fine-grained calcilutite and fault gouge from the Aigion Fault zone, Greece, *C. R. Geoscience* 336 (2004) 445–454, this issue.
- [22] J. Sulem, I. Vardoulakis, H. Ouffroukh, M. Boulon, J. Hans, Experimental characterization of the thermo-poro-mechanical properties of the Aigion fault gouge, *C. R. Geoscience* 336 (2004) 455–466, this issue.
- [23] M.D. Zoback, L.T. Silver, T. Henyey, W. Thatcher, The Cajon Pass Scientific drilling experiment: overview of Phase 1, *Geophys. Res. Lett.* 15 (1988) 933–936.